THE JOURNAL OF PHYSICAL CHEMISTRY C
A JOURNAL OF THE AMERICAN CHEMICAL SOCIETY

pubs.acs.org/JPCC
Article

Photo-Activated, Solid-State Introduction of Luminescent Oxygen Defects into Semiconducting Single-Walled Carbon Nanotubes

Sonja Wieland, Abdurrahman Ali El Yumin, Simon Settele, and Jana Zaumseil*

Cite This: J. Phys. Chem. C 2024, 128, 2012−2021
Read Online

ACCESS | Metrics & More | Article Recommendations | Supporting Information

ABSTRACT: Oxygen defects in semiconducting single-walled carbon nanotubes (SWCNTs) are localized disruptions in the carbon lattice caused by the formation of epoxy or ether groups, commonly through wet-chemical reactions. The associated modifications of the electronic structure can result in luminescent states with emission energies below those of pristine SWCNTs in the near-infrared range, which makes them promising candidates for applications in biosensing and as single-photon emitters. Here, we demonstrate the controlled introduction of luminescent oxygen defects into networks of monochiral (6,5) SWCNTs using a solid-state photocatalytic approach. UV irradiation of SWCNTs on the photoreactive surfaces of the transition metal oxides TiO_x and ZnO_x in the presence of trace amounts of water and oxygen results in the creation of reactive oxygen species that initiate radical reactions with the carbon lattice and the formation of oxygen defects. The created ether-d and epoxide-l defect configurations give rise to two distinct red-shifted emissive features. The chemical and dielectric properties of the photoactive oxides influence the final defect emission properties, with oxygen-functionalized SWCNTs on TiO_x substrates being brighter than those on ZnO_x or pristine SWCNTs on glass. The photoinduced functionalization of nanotubes is further employed to create lateral patterns of oxygen defects in (6,5) SWCNT networks with micrometer resolution and thus spatially controlled defect emission.

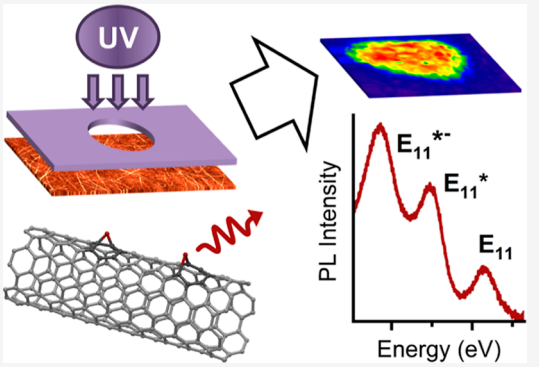

INTRODUCTION

The distinct optical characteristics of semiconducting single-walled carbon nanotubes (SWCNTs) arise from their quasi-one-dimensional structure and the formation of tightly bound excitons upon their excitation.[1,2] The strongest absorption and emission peaks are manifestations of the bright E_{11} exciton. They are observed at diameter-specific energies in the near-infrared range (>900 nm).[3] Of the 16 possible excitons in SWCNTs, only one is bright, with most of the dark excitons lying energetically lower than the bright exciton.[4,5] These dark excitons are one cause of the generally low photoluminescence quantum yield (PLQY) of SWCNTs.[6] Another reason is the fast diffusion of excitons to structural defects or nanotube ends, where they can decay nonradiatively.[7] However, certain defects in the carbon lattice do not act as quenching sites that reduce the PLQY but form lower-lying states that trap mobile excitons and enable radiative decay at longer wavelengths.[8,9] Such luminescent defects can be formed by covalent functionalization, for example, by aryl diazonium chemistry, to create sp^3 carbon atoms within the sp^2 carbon lattice.[10] The resulting defect emission energies (E_{11}* or E_{11}*$^-$) are mainly determined by the binding configuration of the sp^3 carbons,[11] which can be controlled through the choice of synthetic conditions.[12−14] Very similar emission features and, indeed, substantially brighter photoluminescence (PL) are obtained through the reaction of nanotubes with reactive oxygen species (ROS).[15] The properties of the resulting luminescent oxygen defects also depend on the precise binding configuration, with the oxygen being integrated in an ether or epoxide structure (see Figure 1a).[16] Note that the hybridization state of the neighboring C atoms (sp^2 vs sp^3) further influences the defect properties, as observed previously for oxygen- and nitrogen-functionalized SWCNTs.[17−19] Oxygen defects are typically introduced through wet-chemical approaches such as reactions of ozone or hypochlorite in water under UV illumination,[15,16,20,21] but they have also been observed after electron beam evaporation of metal oxides onto SWCNT networks.[22] SWCNTs with luminescent defects can be applied for in vivo imaging in the second biological window,[23,24] optical sensing of biomarkers,[25] and single-photon emission at room temperature.[26]

The creation of luminescent oxygen defects requires less experimental effort than that of sp^3 defects with aryl or alkyl groups. However, unintentional overfunctionalization and

Received: October 23, 2023
Revised: December 17, 2023
Accepted: January 11, 2024
Published: January 24, 2024

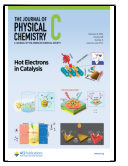

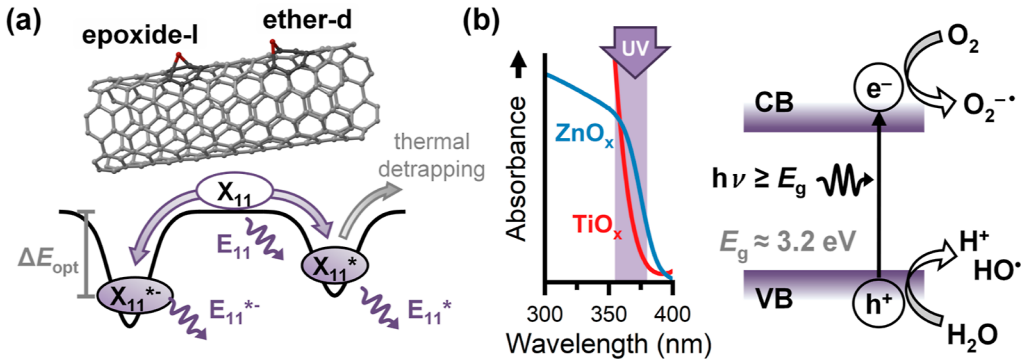

Figure 1. (a) Possible oxygen defect configurations and energetics of different mobile (X_{11}) and localized excitons (X_{11}*$^{-}$ and X_{11}*) in SWCNTs, including the corresponding emission energies (E_{11}, E_{11}*$^{-}$, and E_{11}*) and optical trap depth ΔE_{opt} (energy difference between the mobile exciton and defect emission). (b) Absorption edge spectra of TiO_x and ZnO_x (the UV excitation wavelength range used here is indicated in purple) and schematic of photoinduced creation of ROS by oxidation of water and reduction of oxygen at the surface. CB—conduction band, VB—valence band, and E_g—band gap energy.

degradation of nanotubes during sample processing and storage under ambient conditions might become an issue. Although nanotubes are overall much more stable than typical organic fluorophores, as evidenced by their photostability under laser excitation[27] and high thermal decomposition temperatures (>400 °C),[28] there is significant evidence that (photo)oxidation of SWCNTs can alter their properties in undesired ways.[29,30] Furthermore, Zorn et al. observed that SWCNTs strongly interact with polar silicon dioxide or glass surfaces, which are frequently used as dielectrics or substrates in optoelectronic devices, leading to defect-related broadening and emission sidebands, especially after high-temperature annealing.[29] However, these undesired effects could be avoided by substrate passivation with hexagonal boron nitride (*h*-BN) or cross-linked nonpolar polymers (e.g., BCB). In contrast to that, more reactive or photocatalytic oxidic surfaces in contact with SWCNTs might have a much larger impact on the emission properties of SWCNTs. They may lead to even stronger photodegradation or could be used for the controlled introduction of luminescent defects in predeposited nanotubes.

(6,5) SWCNTs are widely employed for fundamental studies of luminescent defects[31] as they can be sorted in substantial quantities and with high chiral purity through various methods such as selective polymer-wrapping in organic solvents,[6] aqueous two-phase extraction,[32] and gel-chromatography[33] for aqueous dispersions. The high strain in these small-diameter nanotubes increases their reactivity[34] and facilitates defect introduction.[8] Their relatively large band gap of around 1.24 eV enables simple detection of even further red-shifted defect emission features.

The transition metal oxide semiconductors TiO_2 and ZnO are well-known as heterogeneous photocatalysts for the degradation of organic pollutants and the production of renewable fuels and hydrogen by water splitting.[35,36] Excitation with energies greater than their band gap (~3.2 eV), that is, UV irradiation, creates electron−hole pairs that can participate in surface redox reactions, primarily with oxygen and water (see Figure 1b). Under ambient conditions, oxygen is reduced to the reactive superoxide radical anion ($O_2^{\bullet-}$), while water is oxidized to the even more reactive hydroxy radical (HO$^{\bullet}$).[37−39] These ROS readily initiate radical reactions with other molecules, specifically carbon-based materials, directly on the surface.

Here, we demonstrate the photoinduced introduction of luminescent oxygen defects in sparse networks of polymer-sorted (6,5) SWCNTs on TiO_2 and ZnO surfaces upon UV-light exposure in the presence of only trace amounts of water and oxygen. This solid-state photoreaction enables the patterning of luminescent defects in nanotube networks with micrometer resolution. Unlike previous approaches to photopatterning of defects,[40,41] this method is chemical- and solvent-free.

METHODS

Preparation of (6,5) SWCNT Dispersions. Shear-force mixing (Silverson L2/Air, 10,230 rpm) of 50 mg CoMoCat raw material (Sigma-Aldrich, MKCJ7287) in a solution of 65 mg of PFO-BPy (poly[(9,9-dioctylfluorenyl-2,7-diyl)-*alt*-(6,6′-(2,2′-bipyridine))], American Dye Source, Inc., M_w = 40 kg mol^{-1}) in 140 mL of toluene for 72 h at 20 °C was used to prepare nearly monochiral (6,5) SWCNT dispersions, as described previously.[6] Undispersed amorphous carbon and other SWCNT chiralities were separated from the PFO-BPy-wrapped (6,5) SWCNTs by centrifugation (twice, 45 min at 60,000*g*, Beckman Coulter Avanti J26XP centrifuge) and filtration through a syringe filter (Whatman PTFE membrane, pore size 5 μm). To remove excess PFO-BPy, the polymer-rich stock dispersion was vacuum-filtered through a polytetrafluoroethylene membrane (Merck Millipore, JVWP, pore size 0.1 μm). The obtained filter cake was washed three times in 10 mL of toluene at 80 °C for 10 min and redispersed in fresh toluene by bath sonication for 30 min. Absorption (Cary 6000i UV−vis−NIR spectrometer, Varian Inc.) and Raman spectroscopy (InVia Reflex, Renishaw plc) confirmed the chiral purity and low content of the unbound polymer of the (6,5) SWCNT dispersion (see Figure S1, Supporting Information).

Substrate Preparation. Different reactive and unreactive surface layers were prepared on cleaned glass slides (sodium-free aluminum borosilicate glass, Schott AF32 eco). Titanium dioxide layers (9 nm thick) were prepared by annealing a spin-coated organotitanate precursor layer (Solaronix Ti-Nanoxide BL/SC) at 500 °C for 45 min. Zinc oxide layers were deposited by airbrush-spraying a 0.3 molar solution of $Zn(OAc)_2{\cdot}2H_2O$ (Sigma-Aldrich, 99.9%) in methanol onto a heated (200 °C) glass substrate, resulting in 200 nm thick layers. For a passivated surface without any oxidic or hydroxyl groups, the divinyltetramethyl-siloxanebisbenzocyclobutene

https://doi.org/10.1021/acs.jpcc.3c07000
J. Phys. Chem. C 2024, 128, 2012−2021

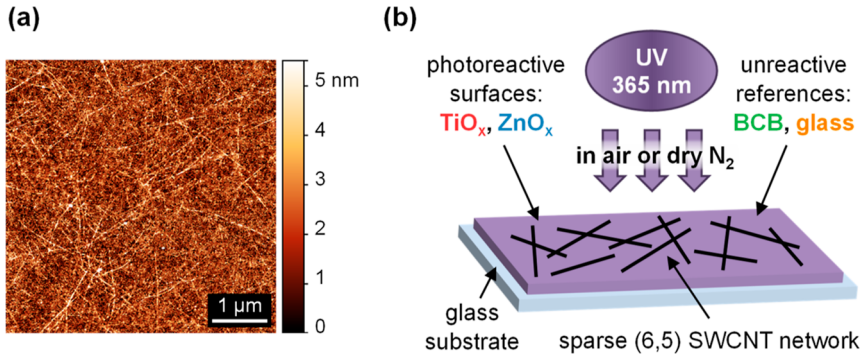

Figure 2. (a) Atomic force micrograph of a sparse SWCNT network on TiO_x. (b) Schematic substrate layout and UV exposure geometry: sparse, spin-coated (6,5) SWCNT networks on a glass substrate coated with different photoactive (TiO_x, ZnO_x) layers and with passivated or unreactive reference (BCB, glass) surfaces.

(BCB) precursor (Cyclotene 3022−35, micro resist technology GmbH) was diluted in a 1:4 ratio in mesitylene, spin-coated, and subsequently cross-linked at 290 °C for 2 min, resulting in 80 nm layers.

All substrates (except BCB-passivated substrates) were treated in a UV/ozone cleaner for 10 min before depositing the (6,5) SWCNTs from toluene dispersion (E_{11} absorbance of 2 at a 1 cm path length) with three consecutive spin-coating steps. Samples were heated at 90 °C for 2 min after each step. Excess PFO-BPy was removed by washing with tetrahydrofuran and 2-propanol and subsequent annealing at 90 °C for 4 min. The deposited (6,5) SWCNTs had an average length of 1.2 ± 0.4 μm and showed network densities of around 10 nanotubes/μm, as determined by atomic force microscopy (AFM, Bruker Dimension Icon, see Figure S2, Supporting Information).

Defect Introduction. The (6,5) SWCNT networks on different surfaces were illuminated with a UV light-emitting diode (SOLIS-365C, Thorlabs, 365 nm, 1.9 mW mm^{-2}) for 2, 15, and 30 min in ambient air or in dry nitrogen (glovebox, H_2O: 0.7 ppm, O_2: <0.1 ppm) or for 15 min with a green light-emitting diode (SOLIS-525C, Thorlabs, 525 nm, 1.4 mW mm^{-2}, together with a 500 nm long-pass filter to exclude unintentional substrate excitation) in dry nitrogen. A fresh substrate was used for each irradiation condition. For the UV exposure series (exposure time-dependent experiments in air and in dry nitrogen), individual substrate pieces were cut from one parent substrate after spin-coating to ensure similar SWCNT densities across the exposure series. All substrates were annealed at 150 °C for 30 min inside the glovebox before illumination. Photopatterning of defects was achieved by exposure to UV light through a 60 μm thick metal shadow mask with holes of 60 μm diameter for 30 min in dry nitrogen.

Optical Characterization. PL spectra were collected with a Princeton Instruments IsoPlane SCT 320 spectrometer in combination with a thermoelectrically cooled InGaAs camera (NIRvana 640ST, Princeton Instruments, 512 × 640 pixels). An 850 nm long-pass filter in front of the spectrometer entrance slit blocked scattered excitation laser light (640 nm, continuous-wave laser diode; OBIS, Coherent). All spectra were averaged over an area of 800 μm^2 through expansion of the laser beam using a plano-convex lens (focal length f = 125 mm) in front of the near-infrared-optimized 20× Olympus objective and vertical binning to remove spot-to-spot variations, as reported elsewhere.[42] Temperature-dependent PL measurements were carried out in a closed-cycle liquid helium-cooled cryostat (Montana Cryostation s50) at high vacuum (<10^{-5} mbar) using a long-working distance, NIR-optimized 50× objective (N.A. 0.42, Mitutoyo) mounted outside the cryostat. PL spectra were corrected for the featureless scattering background of the excitation laser light, for the absorption of optics in the detection path, and for the sensitivity of the detector. They were fitted with three Lorentzian peaks after Jacobian wavelength-to-energy-scale conversion.[43]

Time-correlated single-photon counting (TCSPC) was carried out to determine PL lifetimes using an InGaAs/InP avalanche photodiode (Micro Photon Devices). The SWCNTs were excited at 640 nm with a picosecond-pulsed supercontinuum laser (NKT Photonics SuperK Extreme), and the detection wavelength was selected using a spectrograph (Princeton Instruments Acton SpectraPro SP2358). TCSPC time traces were generated with a counting module (PicoQuant PicoHarp 300) and fitted as biexponential decays with short- and long-lifetime components.

Raman spectra (Renishaw inVia confocal Raman microscope) were collected from 1500 spots across 40 × 70 μm^2 of the nanotube networks using an Olympus 50× short working distance objective under near-resonant excitation at 532 nm. Raman peaks were fitted for each spot with Renishaw Wire 3.4 software using a combination of Lorentzian and Gaussian fit functions. The average values of the D/G^+ ratios were obtained by averaging the ratios obtained from single fits. However, for D-band intensities below 100 counts, i.e., in the case of the TiO_x sample irradiated for 2 min in air, the signal was not sufficient for reliable single-spot fitting, and the D/G^+ ratios were calculated from fits of the averaged Raman spectra instead.

RESULTS AND DISCUSSION

To explore the photoactivated introduction of luminescent oxygen defects into (6,5) SWCNTs on reactive surfaces, semiconducting transition metal oxides that are known for their photocatalytic behavior, such as TiO_2 and ZnO, were chosen, as outlined above. The corresponding oxide layers were formed via spin-coating or spray-coating on glass, followed by annealing (see Methods Section). Nevertheless, they remained mostly amorphous, and the precise stoichiometry may vary; hence, we refer to them as TiO_x and ZnO_x in the following. Clean aluminum borosilicate glass or BCB-passivated glass substrates served as reference samples. Deposition of (6,5) nanotubes by spin-coating from one

https://doi.org/10.1021/acs.jpcc.3c07000
J. Phys. Chem. C 2024, 128, 2012−2021

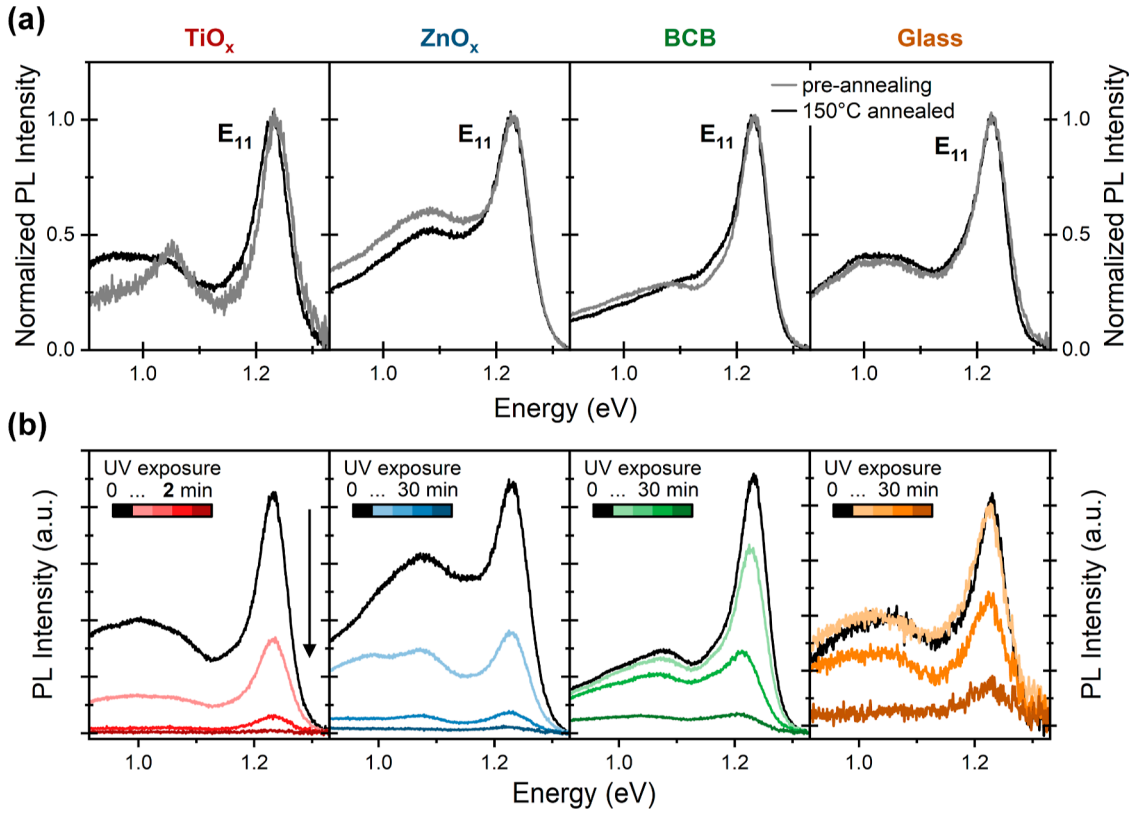

Figure 3. (a) PL spectra of sparse (6,5) SWCNT networks on different substrates and effect of annealing at 150 °C for 30 min in dry nitrogen before illumination. (b) Exposure time-dependent PL spectra of (6,5) SWCNT networks illuminated with UV-light in ambient air (TiO_x: 0, 5, 25, and 120 s; all others: 0, 2, 15, and 30 min).

stock dispersion onto different substrates gave sparse and random networks with similar densities on all surfaces (Figures 2a and S2, Supporting Information). After annealing in nitrogen, these networks were exposed to UV light (365 nm, 3.4 eV) in air or in dry nitrogen for different periods of time, as schematically shown in Figure 2b. We can assume that all SWCNTs within the sparse network are in direct contact with the underlying substrate and, in contrast to dense networks or SWCNT bundles, are equally likely to undergo reactions with reactive species that are created at the oxide surface. Sparse networks further promote effective UV absorption by the underlying reactive oxide as light absorption by SWCNT/PFO-BPy will be negligible.

Before illumination, all as-deposited SWCNT networks (see Figure 3a) exhibited PL spectra with characteristically narrow excitonic E_{11} emission at 1.232 eV and weak, red-shifted sideband features as commonly observed in networks of (6,5) SWCNTs. The sideband contributions to the PL signal increased from nonpolar BCB to polar substrates and from nonreactive to reactive oxide surfaces, as expected.[29,44] These sidebands have been assigned to momentum-forbidden dark excitons coupling to phonons and to shallow extrinsic defects of the (6,5) SWCNT lattice due to interaction with reactive groups on mostly polar surfaces.[45−47] The additional feature observed at 1.051 eV for the TiO_x sample most likely corresponds to SWCNT trion (charged exciton) emission due to slight p-doping by the oxide.[42] The relatively strong sideband for (6,5) SWCNTs even on BCB-passivated samples probably results from the low network density. All nanotubes were in direct contact with the underlying substrate, and their remaining surface was exposed to the environment. Note that even the surface of polymer-wrapped nanotubes is only partially covered by polymer (appr. 10%).[48] Consequently, these SWCNTs were more susceptible to any unwanted reactions than nanotubes in dense networks or bundles.

Figure 3a further shows the impact of mild annealing (30 min at 150 °C) of the samples in the dry nitrogen atmosphere of a glovebox. This annealing step was performed to remove adsorbed water from the SWCNTs and the substrate surfaces as much as possible and to ensure reproducible starting points for all samples prior to UV exposure. Importantly, this treatment did not significantly alter the emission properties or the Raman spectra (specifically the intensity of the defect-related D-mode and the corresponding D/G^+ ratios as a metric for defect density,[49,50] see Figure S3, Supporting Information) of the SWCNT networks. For nanotubes on the TiO_x surface, the trion emission disappeared and a featureless sideband similar to that on glass emerged, while the Raman D/G^+ ratio increased slightly. While interactions with the polar substrate surface could contribute to the PL spectral shape, slight changes might also be indicative of a thermally driven defect introduction in SWCNTs on highly reactive TiO_x surfaces.

When these SWCNT networks were exposed to UV light in air, that is, in the presence of plenty of oxygen and water, their PL was almost completely quenched within less than 30 min. For nanotube networks on the highly reactive TiO_x surface, the PL vanished completely after only 2 min of UV illumination in air (see Figures 3b and S4a, Supporting Information). The emission from nanotubes on ZnO_x was quenched slower than on TiO_x, but still much faster than for those on glass or BCB. The rapid increase of the Raman D/G^+ ratios up to 0.5 upon UV illumination in air (Figure S4b,c, Supporting Information)

https://doi.org/10.1021/acs.jpcc.3c07000
J. Phys. Chem. C 2024, 128, 2012−2021

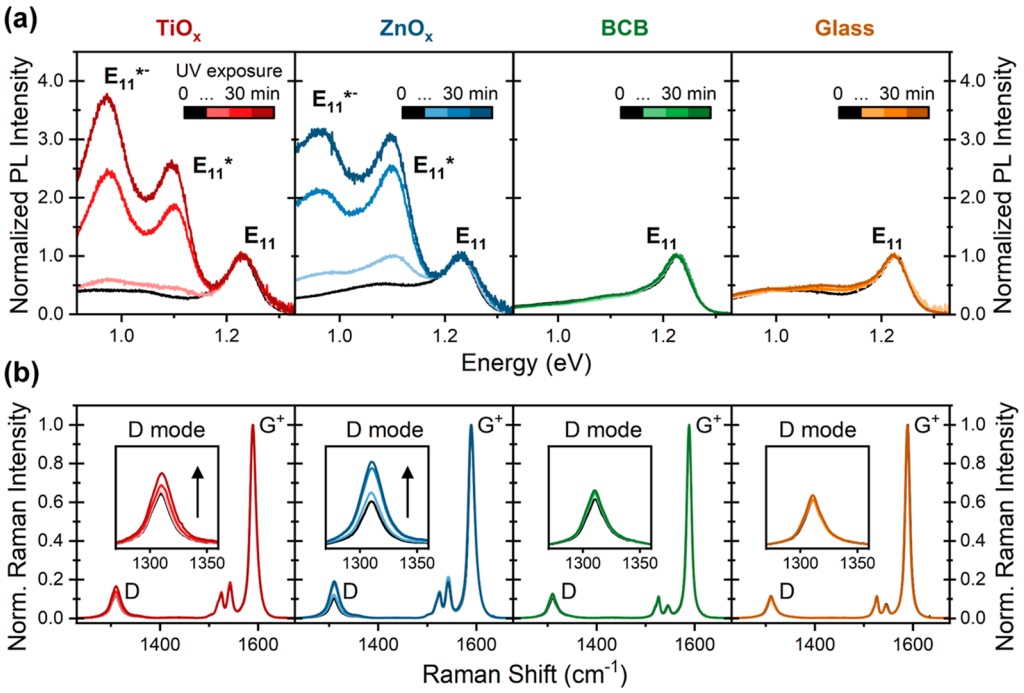

Figure 4. Evolution of PL spectra normalized to E_{11} after UV exposure for 0, 2, 15, and 30 min in dry nitrogen (glovebox). (b) Resonant Raman spectra (excitation at 532 nm) normalized to the G^+ mode show the increase of the defect-related D-mode with illumination for reactive surfaces.

indicates the immediate creation of structural defects in the carbon lattice. For nanotubes on both TiO_x and ZnO_x, we can assume that ROS such as $O_2^{\bullet-}$ and $HO^{\bullet}$ were formed from oxygen and water, respectively, upon photoexcitation of the oxide.[35,36] These ROS directly attacked the carbon lattice of the nanotubes and created a large number of defects that led to nonradiative decay and PL quenching. The direct generation of ROS from air through UV excitation of oxygen as demonstrated by Xhyliu et al.[51] for irradiation with 254 nm (4.88 eV) light is unlikely since the energy (3.4 eV) of the 365 nm light used here is too low for this process but well above the bandgap of TiO_x and ZnO_x (optical band gaps of 3.19 eV for ZnO_x and 3.29 eV for TiO_x as determined by Tauc plots[52]). The much slower photodegradation of nanotubes on BCB and glass further highlights the important photocatalytic role of the oxides. PL quenching after several minutes of illumination is, however, consistent with reports by Larson et al., who proposed singlet oxygen sensitization or the formation of superoxide from oxygen through the direct excitation of the nanotubes in the UV to visible range as a cause for photodegradation.[30]

Importantly, at no point do the spectral features of luminescent oxygen defects appear for nanotubes on any of the substrates. Either the sp^2 lattice is destroyed too quickly in too many places to allow for defect PL to be observed, or the type of defect formation is different under these conditions. ROS could initiate a chain reaction with excess oxygen, creating higher-oxidized species, as previously observed for less-extended aromatic systems.[36] This should result in sidewall damage similar to the reaction products of superoxide treatment and oxidative cutting of SWCNTs, where, e.g., hydroxyl, aldehyde, ketone, and carboxylic acid defects act as exciton quenching sites and hence lead to a reduction of the PL intensity.[30,53,54]

Clearly, the number of possible ROS produced by UV illumination must be reduced substantially to create a limited number of luminescent defects (only a few per micrometer) instead of damaging the entire carbon lattice. A much lower concentration of oxygen and water surrounding the nanotubes can be achieved by performing UV exposure inside a dry nitrogen glovebox. The previously described annealing step should also reduce adsorbed water or oxygen on the photoactive substrates; however, neither can be fully removed from a polar surface under these conditions (that is, not in high vacuum, limited temperature range). Residual parts per million amounts of both oxygen and water will always be present.

Figure 4a shows the evolution of the PL spectra (normalized to E_{11}) of (6,5) SWCNT networks on different substrates after UV illumination for 2, 15, and 30 min in dry nitrogen. The PL spectra for nanotubes on BCB and glass did not change significantly in shape or intensity (see also Figure S5a, Supporting Information). Their D/G^+ ratios also remained nearly constant (see Figure 4b). This indifference of SWCNTs on BCB and glass to UV exposure is in stark contrast to nanotubes on the photoreactive oxide surfaces. After exposure of (6,5) nanotubes on both TiO_x and ZnO_x, two additional red-shifted emission peaks, denoted here as E_{11}^* (1.10 eV, 1130 nm) and E_{11}^{*-} (0.95−0.97 eV, 1280−1300 nm), appeared (see Figure S6, Supporting Information for extended energy range spectra). The Raman D/G^+ ratios increased noticeably but not to a degree that would indicate severe lattice damage.

The intensities of the E_{11}^* and E_{11}^{*-} emissions relative to the E_{11} emission differed between the two photoreactive oxides. UV-illuminated nanotubes on ZnO_x exhibited broader defect emission peaks [full width at half-maximum (fwhm) E_{11}^{*-}: 214 meV, E_{11}^*: 96 meV] than SWCNTs on TiO_x (fwhm E_{11}^{*-}: 163 meV, E_{11}^*: 86 meV), possibly caused by the higher dipolar disorder of the rough ZnO_x surface.[44,55] The overall PL intensity was actually enhanced for nanotube networks on TiO_x, it decreased for nanotubes on ZnO_x, and remained nearly constant for BCB substrates (see Figure S5,

https://doi.org/10.1021/acs.jpcc.3c07000
J. Phys. Chem. C 2024, 128, 2012−2021

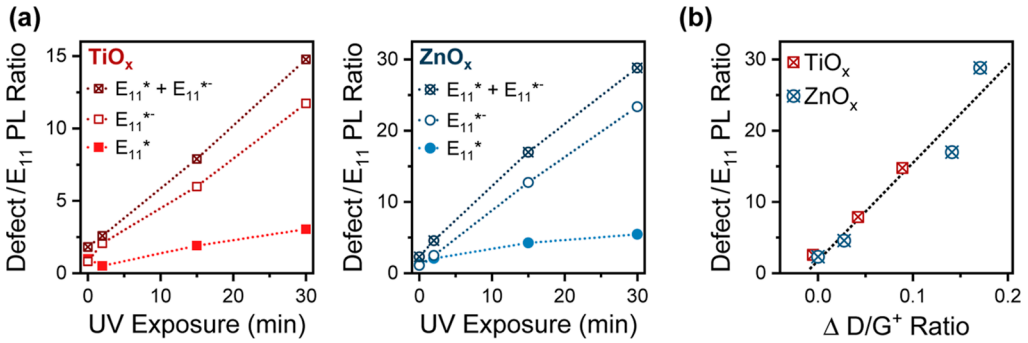

Figure 5. (a) Increase in fitted relative defect PL area with UV exposure time in dry nitrogen for TiO_x (left) and ZnO_x (right). Note that the value at 0 min of exposure time corresponds to the intrinsic defect-related sideband emission of the pristine SWCNTs. (b) Linear correlation of relative defect PL versus the corresponding Raman D/G$^+$ ratio change induced by UV illumination of sparse SWCNT networks on photoactive surfaces (TiO_x and ZnO_x) in dry nitrogen.

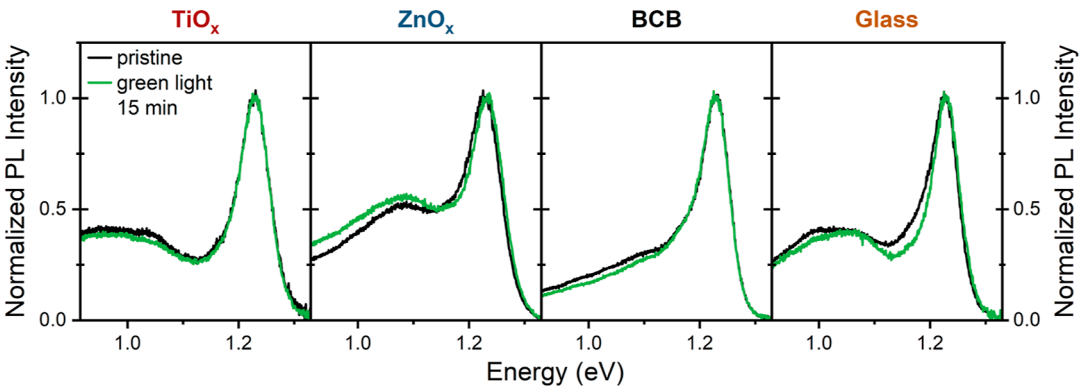

Figure 6. PL spectra of sparse SWCNT networks on different surfaces before and after 15 min of illumination with green light (525 nm) in dry nitrogen.

Supporting Information). The defect emission intensities relative to E_{11} increased with reaction time (see Figure 5a), while the absolute E_{11} intensities decreased due to the trapping of mobile excitons at the defect sites. The almost linear increase of defects (see Figure 5a) with UV illumination time suggests that the reaction was limited by the number of formed ROS and no autocatalytic process or chain reaction was initiated. As shown in Figure 5b, the defect emission to E_{11} ratio also increased linearly with the differential Raman D/G$^+$ ratio for nanotubes on both TiO_x and ZnO_x, as observed before for luminescent sp^3 defects,[12,56] with the slope being independent of the oxide type.

The two main defect emission features E_{11}* and the more red-shifted E_{11}*$^-$ exhibit optical trap depths of 137 and 268 meV on TiO_x and 140 and 288 meV on ZnO_x, respectively. These values are comparable to the trap depths of the ether-d (135 meV) and epoxide-l (300 meV) defect configurations observed by Ma et al. after electron beam evaporation of oxides onto SWCNTs[16] and were also proposed for defects created by the reaction of nanotubes with ozone or hypochlorite under UV illumination.[15,22,23] Hence, we assume that these or similar luminescent oxygen defects are formed by the reaction of ROS with the (6,5) nanotube lattice. The photoexcitation of TiO_x and ZnO_x by UV light should result in the formation of ROS in the vicinity of the nanotubes but in very low numbers due to the very limited concentrations of water or oxygen. The contributions of the two different types of initially formed ROS, i.e., the superoxide radical anion and the hydroxy radical, cannot be distinguished directly. However, the formation of hydroxy radicals from water seems most likely as adsorbed water on polar surfaces is very difficult to remove. The hydroxy radical is also known to be more reactive.[37−39]

Previous reports have suggested that the bandgap excitation of nanotubes could result in electron transfer and photo-induced reactions to form luminescent defects without the need of high-energy UV light or the presence of photoreactive surfaces.[30,57] As shown above, there is little or no change in the emission spectra of (6,5) SWCNTs when exposed to UV light on glass or BCB surfaces in dry nitrogen. When exposed to UV light in air, only PL quenching occurs over time. Nevertheless, we also tested whether luminescent defects could be introduced to SWCNTs on reactive surfaces when exposed to visible light that should not lead to any photoexcitation of TiO_x or ZnO_x but is above the bandgap and indeed excites the E_{22} transition (575 nm, 2.16 eV) and phonon sideband of (6,5) nanotubes (see Figure S1b, Supporting Information). A set of SWCNT network samples was exposed to green light (525 nm, 2.36 eV) with an intensity comparable to that of the UV exposure. No changes in the emission spectra on any of the substrates were observed (see Figure 6), corroborating the role of the direct photoexcitation of TiO_x or ZnO_x for the introduction of luminescent oxygen defects in SWCNTs.

To learn more about the properties of these photoinduced defect states and compare them to oxygen defects created by other methods, their averaged PL lifetimes τ_{avg} were determined by TCSPC (Figure S7 and Table S1, Supporting Information). The luminescent defects in SWCNTs on TiO_x showed longer PL lifetimes (E_{11}*$^-$ 60 ps, E_{11}* 26 ps)

https://doi.org/10.1021/acs.jpcc.3c07000
J. Phys. Chem. C 2024, 128, 2012−2021

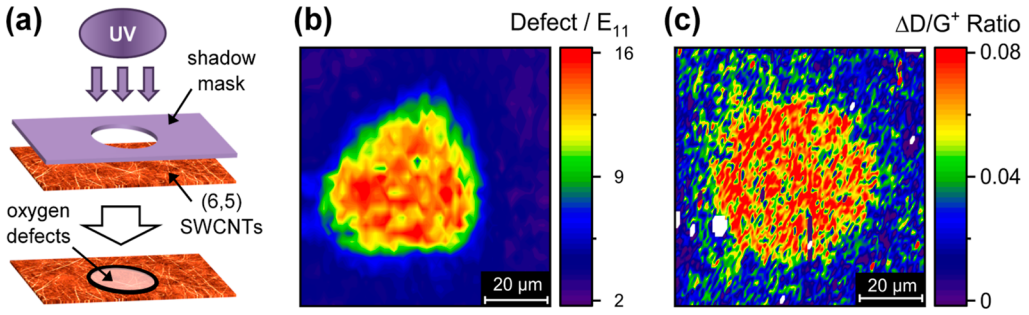

Figure 7. (a) Schematic defect patterning process of (6,5) SWCNT networks on TiO_x surface by UV exposure (30 min) through a shadow mask in dry nitrogen. Visualization of the induced luminescent defect pattern by (b) combined defect/E_{11} PL ratio map and (c) Raman D/G^+ ratio map.

compared to those on ZnO_x (E_{11}^{*-} 42 ps, E_{11}^* 25 ps), suggesting an impact of additional nonradiative decay paths such as multiphonon decay (MPD) and electronic-to-vibrational energy transfer to the substrate.[58,59] The longer PL lifetimes of the E_{11}^{*-} defects compared to those of the E_{11}^* defects correlated with their different optical trap depths (see above), as expected.[59] Note that the lifetimes measured for these sparse networks on substrates were very short compared to defect lifetimes of functionalized nanotubes in dispersion due to increased nonradiative decay paths, as observed previously. For example, Zorn et al. reported amplitude-averaged E_{11}^* defect lifetimes of 222 ps in dispersion versus 32−60 ps when deposited on substrates.[29]

Furthermore, temperature-dependent PL measurements and defect/E_{11} intensity ratios (see Figure S8a,b, Supporting Information) can help establish the thermal trap depth. The data collected from (6,5) SWCNT networks between 25 and 300 K on TiO_x and ZnO_x samples after 30 min of UV exposure in dry nitrogen showed the expected increase of defect emission with temperature due to increasing thermal energy to overcome potential barriers for mobile excitons around the defect sites, as reported by Kim et al.[60] A further increase in temperature should result in a reduction of the relative defect intensity as thermal detrapping of excitons from the defect states starts to play a role. From this temperature range, the thermal trap depths can be extracted using van't Hoff plots of the temperature-dependent defect emission intensity relative to the E_{11} emission[61] (see Figure S8c, Supporting Information). On TiO_x, the extracted thermal trap depths were 100 and 36 meV for E_{11}^* and E_{11}^{*-} defects, respectively, while on ZnO_x, the thermal trap depth was found to be only 14 meV for E_{11}^*. The trap depth for E_{11}^{*-} could not be determined in the experimentally accessible temperature range (see Table S1, Supporting Information). Note that these thermal trap depths are comparable to those previously reported by Kim et al. for oxygen defects (24 meV) with similar optical trap depths.[61] However, thermal trap depths of luminescent defects also depend on defect density,[61] defect distribution, and surface polarity with MPD as a competing process.[59] A conclusive explanation for the trap depths of the O-defects introduced on ZnO_x and on TiO_x is not possible at this point.

Finally, the selective introduction of luminescent oxygen defects in nanotube networks through UV illumination enables the creation of patterns of enhanced and red-shifted defect emission with a high spatial resolution using suitable masks. Due to the necessary requirement of a dry nitrogen environment for UV exposure, we were limited to the use of a metal shadow mask with 60 μm diameter holes. The mask was placed on top of a network of (6,5) SWCNTs on a TiO_x substrate and illuminated for 30 min, as schematically shown in Figure 7a. Subsequently, a corresponding spot of defect emission could be imaged by PL microscopy (Figure 7b). The defect to E_{11} emission ratio shows a very clear contrast, while the increase of the total PL signal was less well-defined (see Figure S9, Supporting Information) due to the inhomogeneous distribution of SWCNTs and overall variations of PL intensity. Similar to the defect emission, the distribution of defects after illumination can be visualized by confocal Raman microscopy. A map of the D/G^+ signal ratio (see Figure 7c) also shows a circular pattern with an approximate diameter of 50−55 μm, representing the functionalized nanotubes. Note that the PL and Raman images were not acquired from the same spot. The slightly different shapes and diameters are most likely the result of shadow effects due to the mask thickness of 60 μm. We believe that the size of the patterned area could be reduced further using a direct UV laser writer or a mask aligner under inert conditions. Due to the highly local nature of the reaction, the spatial resolution should be limited only by the illumination wavelength (365 nm) and the illumination optics. It should thus be possible to reach a resolution of a few hundred nanometers.

CONCLUSIONS

We have demonstrated the direct UV light-induced formation of luminescent oxygen defects in networks of (6,5) SWCNTs on photocatalytic TiO_x and ZnO_x surfaces under nominally inert conditions in a dry nitrogen glovebox. The reaction occurs in the solid state and does not require any solvents, additional reagents, or post-treatment. We propose that water and/or oxygen adsorbed on the SWCNTs or substrate surface are oxidized/reduced by the photoexcited TiO_x and ZnO_x to form ROS that readily react with the carbon lattice of the nanotubes to form luminescent oxygen defects. Two types of emissive defects were formed, whose emission wavelengths correlate well with previously reported ether-d and epoxide-l oxygen defect configurations. The defect PL intensities varied significantly between the reactive surfaces, with defects in nanotubes on TiO_x leading to overall brighter PL intensities compared to those of nonilluminated SWCNTs and those irradiated on ZnO_x. We assume that other photoreactive oxides with different bandgaps and valence and conduction band energies (e.g., WO_3 and In_2O_3)[62] could lead to different reactions and thus defects or defect densities depending on the preferential formation of hydroxy or superoxide anion radicals. Importantly, UV exposure in ambient air led to fast degradation of SWCNTs even on nonreactive BCB and glass substrates instead of the creation of luminescent defects, thus

https://doi.org/10.1021/acs.jpcc.3c07000
J. Phys. Chem. C 2024, 128, 2012−2021

highlighting the importance of limiting the concentration of oxygen and water.

We applied the photoinduced formation of bright oxygen defects to create controlled emission patterns in nanotube networks by using a shadow mask during illumination. This simple approach could enable direct UV laser writing or photolithographic patterning of oxygen defects into SWCNT networks under inert conditions without the need for any photoresist or developer. However, our results also highlight the potential problems of photoreactive layers of TiO_x or ZnO_x and possibly other materials that are part of optoelectronic devices with SWCNTs as active components. Their interactions at the interface during processing and operation (e.g., photodiodes or photovoltaic cells) may lead to unintended and undesired changes in their electronic and optical properties and, thus, may affect short- and long-term device performance.

■ ASSOCIATED CONTENT

Supporting Information

The Supporting Information is available free of charge at https://pubs.acs.org/doi/10.1021/acs.jpcc.3c07000.

Raman and absorption spectra of pristine (6,5) SWCNT dispersions, atomic force and optical micrographs of substrate surfaces with nanotube networks, Raman spectra of annealed SWCNT networks, PL quenching and Raman D/G$^+$ ratio increase upon UV exposure in air, absolute PL spectra of SWCNT networks after UV exposure in dry nitrogen, extended energy-range defect PL spectra, TCSPC measurements of defect PL lifetimes, temperature-dependent PL spectra of functionalized SWCNTs, and PL maps (relative and absolute) of patterned luminescent defects (PDF)

■ AUTHOR INFORMATION

Corresponding Author

Jana Zaumseil − *Institute for Physical Chemistry, Universität Heidelberg, D-69120 Heidelberg, Germany;* orcid.org/0000-0002-2048-217X; Email: zaumseil@uni-heidelberg.de

Authors

Sonja Wieland − *Institute for Physical Chemistry, Universität Heidelberg, D-69120 Heidelberg, Germany*

Abdurrahman Ali El Yumin − *Institute for Physical Chemistry, Universität Heidelberg, D-69120 Heidelberg, Germany*

Simon Settele − *Institute for Physical Chemistry, Universität Heidelberg, D-69120 Heidelberg, Germany;* orcid.org/0000-0002-0082-2587

Complete contact information is available at: https://pubs.acs.org/10.1021/acs.jpcc.3c07000

Notes

The authors declare no competing financial interest.

■ ACKNOWLEDGMENTS

This project has received funding from the European Research Council (ERC) under the European Union's Horizon 2020 research and innovation programme (grant agreement no. 817494, "TRIFECTs").

■ REFERENCES

(1) Spataru, C. D.; Ismail-Beigi, S.; Benedict, L. X.; Louie, S. G. Excitonic Effects and Optical Spectra of Single-Walled Carbon Nanotubes. *Phys. Rev. Lett.* **2004**, *92*, 077402.

(2) Wang, F.; Dukovic, G.; Brus, L. E.; Heinz, T. F. The Optical Resonances in Carbon Nanotubes Arise from Excitons. *Science* **2005**, *308*, 838−841.

(3) Lefebvre, J.; Fraser, J. M.; Finnie, P.; Homma, Y. Photoluminescence from an Individual Single-Walled Carbon Nanotube. *Phys. Rev. B: Condens. Matter Mater. Phys.* **2004**, *69*, 075403.

(4) Mortimer, I. B.; Nicholas, R. J. Role of Bright and Dark Excitons in the Temperature-Dependent Photoluminescence of Carbon Nanotubes. *Phys. Rev. Lett.* **2007**, *98*, 027404.

(5) Amori, A. R.; Hou, Z.; Krauss, T. D. Excitons in Single-Walled Carbon Nanotubes and Their Dynamics. *Annu. Rev. Phys. Chem.* **2018**, *69*, 81−99.

(6) Graf, A.; Zakharko, Y.; Schießl, S. P.; Backes, C.; Pfohl, M.; Flavel, B. S.; Zaumseil, J. Large Scale, Selective Dispersion of Long Single-Walled Carbon Nanotubes with High Photoluminescence Quantum Yield by Shear Force Mixing. *Carbon* **2016**, *105*, 593−599.

(7) Hertel, T.; Himmelein, S.; Ackermann, T.; Stich, D.; Crochet, J. Diffusion Limited Photoluminescence Quantum Yields in 1-D Semiconductors: Single-Wall Carbon Nanotubes. *ACS Nano* **2010**, *4*, 7161−7168.

(8) Piao, Y.; Meany, B.; Powell, L. R.; Valley, N.; Kwon, H.; Schatz, G. C.; Wang, Y. Brightening of Carbon Nanotube Photoluminescence through the Incorporation of sp^3 Defects. *Nat. Chem.* **2013**, *5*, 840−845.

(9) Gifford, B. J.; Kilina, S.; Htoon, H.; Doorn, S. K.; Tretiak, S. Controlling Defect-State Photophysics in Covalently Functionalized Single-Walled Carbon Nanotubes. *Acc. Chem. Res.* **2020**, *53*, 1791−1801.

(10) Brozena, A. H.; Kim, M.; Powell, L. R.; Wang, Y. Controlling the Optical Properties of Carbon Nanotubes with Organic Colour-Centre Quantum Defects. *Nat. Rev. Chem.* **2019**, *3*, 375−392.

(11) Saha, A.; Gifford, B. J.; He, X.; Ao, G.; Zheng, M.; Kataura, H.; Htoon, H.; Kilina, S.; Tretiak, S.; Doorn, S. K. Narrow-Band Single-Photon Emission through Selective Aryl Functionalization of Zigzag Carbon Nanotubes. *Nat. Chem.* **2018**, *10*, 1089−1095.

(12) Settele, S.; Berger, F. J.; Lindenthal, S.; Zhao, S.; El Yumin, A. A.; Zorn, N. F.; Asyuda, A.; Zharnikov, M.; Högele, A.; Zaumseil, J. Synthetic Control over the Binding Configuration of Luminescent sp^3-Defects in Single-Walled Carbon Nanotubes. *Nat. Commun.* **2021**, *12*, 2119.

(13) Yu, B.; Naka, S.; Aoki, H.; Kato, K.; Yamashita, D.; Fujii, S.; Kato, Y. K.; Fujigaya, T.; Shiraki, T. Ortho-Substituted Aryldiazonium Design for the Defect Configuration-Controlled Photoluminescent Functionalization of Chiral Single-Walled Carbon Nanotubes. *ACS Nano* **2022**, *16*, 21452−21461.

(14) Wang, P.; Fortner, J.; Luo, H.; Kłos, J.; Wu, X.; Qu, H.; Chen, F.; Li, Y.; Wang, Y. Quantum Defects: What Pairs with the Aryl Group When Bonding to the sp^2 Carbon Lattice of Single-Wall Carbon Nanotubes? *J. Am. Chem. Soc.* **2022**, *144*, 13234−13241.

(15) Ghosh, S.; Bachilo, S. M.; Simonette, R. A.; Beckingham, K. M.; Weisman, R. B. Oxygen Doping Modifies near-Infrared Band Gaps in Fluorescent Single-Walled Carbon Nanotubes. *Science* **2010**, *330*, 1656−1659.

(16) Ma, X.; Adamska, L.; Yamaguchi, H.; Yalcin, S. E.; Tretiak, S.; Doorn, S. K.; Htoon, H. Electronic Structure and Chemical Nature of Oxygen Dopant States in Carbon Nanotubes. *ACS Nano* **2014**, *8*, 10782−10789.

(17) Zhang, K.; Wang, J.; Zou, J.; Cai, W.; Zhang, Q. Low Excitation of Raman D-Band in [2 + 1] Cycloaddition Functionalized Single-Walled Carbon Nanotubes. *Carbon* **2018**, *138*, 188−196.

(18) Setaro, A.; Adeli, M.; Glaeske, M.; Przyrembel, D.; Bisswanger, T.; Gordeev, G.; Maschietto, F.; Faghani, A.; Paulus, B.; Weinelt, M.; Arenal, R.; Haag, R.; Reich, S. Preserving π-Conjugation in Covalently Functionalized Carbon Nanotubes for Optoelectronic Applications. *Nat. Commun.* **2017**, *8*, 14281.

(19) Hayashi, K.; Niidome, Y.; Shiga, T.; Yu, B.; Nakagawa, Y.; Janas, D.; Fujigaya, T.; Shiraki, T. Azide Modification Forming Luminescent sp^2 Defects on Single-Walled Carbon Nanotubes for near-Infrared Defect Photoluminescence. *Chem. Commun.* **2022**, *58*, 11422−11425.
(20) Eremin, T.; Eremina, V.; Svirko, Y.; Obraztsov, P. Over Two-Fold Photoluminescence Enhancement from Single-Walled Carbon Nanotubes Induced by Oxygen Doping. *Nanomaterials* **2023**, *13*, 1561.
(21) Iizumi, Y.; Yudasaka, M.; Kim, J.; Sakakita, H.; Takeuchi, T.; Okazaki, T. Oxygen-Doped Carbon Nanotubes for near-Infrared Fluorescent Labels and Imaging Probes. *Sci. Rep.* **2018**, *8*, 6272.
(22) Ma, X.; Baldwin, J. K. S.; Hartmann, N. F.; Doorn, S. K.; Htoon, H. Solid-State Approach for Fabrication of Photostable, Oxygen-Doped Carbon Nanotubes. *Adv. Funct. Mater.* **2015**, *25*, 6157−6164.
(23) Lin, C.-W.; Bachilo, S. M.; Zheng, Y.; Tsedev, U.; Huang, S.; Weisman, R. B.; Belcher, A. M. Creating Fluorescent Quantum Defects in Carbon Nanotubes Using Hypochlorite and Light. *Nat. Commun.* **2019**, *10*, 2874.
(24) Mandal, A. K.; Wu, X.; Ferreira, J. S.; Kim, M.; Powell, L. R.; Kwon, H.; Groc, L.; Wang, Y.; Cognet, L. Fluorescent sp^3 Defect-Tailored Carbon Nanotubes Enable NIR-II Single Particle Imaging in Live Brain Slices at Ultra-Low Excitation Doses. *Sci. Rep.* **2020**, *10*, 5286.
(25) Kim, M.; Chen, C.; Wang, P.; Mulvey, J. J.; Yang, Y.; Wun, C.; Antman-Passig, M.; Luo, H.-B.; Cho, S.; Long-Roche, K.; et al. Detection of Ovarian Cancer Via the Spectral Fingerprinting of Quantum-Defect-Modified Carbon Nanotubes in Serum by Machine Learning. *Nat. Biomed. Eng.* **2022**, *6*, 267−275.
(26) Ma, X.; Hartmann, N. F.; Baldwin, J. K. S.; Doorn, S. K.; Htoon, H. Room-Temperature Single-Photon Generation from Solitary Dopants of Carbon Nanotubes. *Nat. Nanotechnol.* **2015**, *10*, 671.
(27) Heller, D. A.; Baik, S.; Eurell, T. E.; Strano, M. S. Single-Walled Carbon Nanotube Spectroscopy in Live Cells: Towards Long-Term Labels and Optical Sensors. *Adv. Mater.* **2005**, *17*, 2793−2799.
(28) Miyata, Y.; Mizuno, K.; Kataura, H. Purity and Defect Characterization of Single-Wall Carbon Nanotubes Using Raman Spectroscopy. *J. Nanomater.* **2011**, *2011*, 786763.
(29) Zorn, N. F.; Settele, S.; Zhao, S.; Lindenthal, S.; El Yumin, A. A.; Wedl, T.; Li, H.; Flavel, B. S.; Högele, A.; Zaumseil, J. Near-Intrinsic Photo- and Electroluminescence from Single-Walled Carbon Nanotube Thin Films on BCB-Passivated Surfaces. *Adv. Opt. Mater.* **2023**, *11*, 2300236.
(30) Larson, B. W.; Thurman, K. A.; Kang, H. S.; Ferguson, A. J.; Blackburn, J. L.; Steger, M. Arresting Photodegradation in Semiconducting Single-Walled Carbon Nanotube Thin Films. *ACS Appl. Nano Mater.* **2022**, *5*, 3502−3511.
(31) Arias, D. H.; Sulas-Kern, D. B.; Hart, S. M.; Kang, H. S.; Hao, J.; Ihly, R.; Johnson, J. C.; Blackburn, J. L.; Ferguson, A. J. Effect of Nanotube Coupling on Exciton Transport in Polymer-Free Monochiral Semiconducting Carbon Nanotube Networks. *Nanoscale* **2019**, *11*, 21196−21206.
(32) Li, H.; Gordeev, G.; Garrity, O.; Reich, S.; Flavel, B. S. Separation of Small-Diameter Single-Walled Carbon Nanotubes in One to Three Steps with Aqueous Two-Phase Extraction. *ACS Nano* **2019**, *13*, 2567−2578.
(33) Liu, H.; Nishide, D.; Tanaka, T.; Kataura, H. Large-Scale Single-Chirality Separation of Single-Wall Carbon Nanotubes by Simple Gel Chromatography. *Nat. Commun.* **2011**, *2*, 309.
(34) Banerjee, S.; Wong, S. S. Demonstration of Diameter-Selective Reactivity in the Sidewall Ozonation of SWNTs by Resonance Raman Spectroscopy. *Nano Lett.* **2004**, *4*, 1445−1450.
(35) Nosaka, Y.; Nosaka, A. Y. Generation and Detection of Reactive Oxygen Species in Photocatalysis. *Chem. Rev.* **2017**, *117*, 11302−11336.
(36) Samadi, M.; Zirak, M.; Naseri, A.; Khorashadizade, E.; Moshfegh, A. Z. Recent Progress on Doped ZnO Nanostructures for Visible-Light Photocatalysis. *Thin Solid Films* **2016**, *605*, 2−19.
(37) Mattila, H.; Khorobrykh, S.; Havurinne, V.; Tyystjärvi, E. Reactive Oxygen Species: Reactions and Detection from Photosynthetic Tissues. *J. Photochem. Photobiol., B* **2015**, *152*, 176−214.
(38) Hsieh, H.-S.; Zepp, R. G. Reactivity of Graphene Oxide with Reactive Oxygen Species (Hydroxyl Radical, Singlet Oxygen, and Superoxide Anion). *Environ. Sci.: Nano* **2019**, *6*, 3734−3744.
(39) Armstrong, D. A.; Huie, R. E.; Lymar, S.; Koppenol, W. H.; Merényi, G.; Neta, P.; Stanbury, D. M.; Steenken, S.; Wardman, P. Standard Electrode Potentials Involving Radicals in Aqueous Solution: Inorganic Radicals. *BioInorg. React. Mech.* **2013**, *9*, 59−61.
(40) Huang, Z.; Powell, L. R.; Wu, X.; Kim, M.; Qu, H.; Wang, P.; Fortner, J. L.; Xu, B.; Ng, A. L.; Wang, Y. Photolithographic Patterning of Organic Color-Centers. *Adv. Mater.* **2020**, *32*, 1906517.
(41) Gordeev, G.; Rosenkranz, T.; Hennrich, F.; Reich, S.; Krupke, R. Light Control over Chirality Selective Functionalization of Substrate Supported Carbon Nanotubes. *J. Phys. Chem. C* **2022**, *126*, 9803−9812.
(42) Wieland, S.; El Yumin, A. A.; Gotthardt, J. M.; Zaumseil, J. Impact of Dielectric Environment on Trion Emission from Single-Walled Carbon Nanotube Networks. *J. Phys. Chem. C* **2023**, *127*, 3112−3122.
(43) Mooney, J.; Kambhampati, P. Get the Basics Right: Jacobian Conversion of Wavelength and Energy Scales for Quantitative Analysis of Emission Spectra. *J. Phys. Chem. Lett.* **2013**, *4*, 3316−3318.
(44) Noé, J. C.; Nutz, M.; Reschauer, J.; Morell, N.; Tsioutsios, I.; Reserbat-Plantey, A.; Watanabe, K.; Taniguchi, T.; Bachtold, A.; Högele, A. Environmental Electrometry with Luminescent Carbon Nanotubes. *Nano Lett.* **2018**, *18*, 4136−4140.
(45) Kadria-Vili, Y.; Bachilo, S. M.; Blackburn, J. L.; Weisman, R. B. Photoluminescence Side Band Spectroscopy of Individual Single-Walled Carbon Nanotubes. *J. Phys. Chem. C* **2016**, *120*, 23898−23904.
(46) Blackburn, J. L.; Holt, J. M.; Irurzun, V. M.; Resasco, D. E.; Rumbles, G. Confirmation of K-Momentum Dark Exciton Vibronic Sidebands Using ^{13}C-Labeled, Highly Enriched (6,5) Single-Walled Carbon Nanotubes. *Nano Lett.* **2012**, *12*, 1398−1403.
(47) Lüttgens, J. M.; Berger, F. J.; Zaumseil, J. Population of Exciton-Polaritons via Luminescent sp^3 Defects in Single-Walled Carbon Nanotubes. *ACS Photonics* **2021**, *8*, 182−193.
(48) Shea, M. J.; Mehlenbacher, R. D.; Zanni, M. T.; Arnold, M. S. Experimental Measurement of the Binding Configuration and Coverage of Chirality-Sorting Polyfluorenes on Carbon Nanotubes. *J. Phys. Chem. Lett.* **2014**, *5*, 3742−3749.
(49) Sebastian, F. L.; Zorn, N. F.; Settele, S.; Lindenthal, S.; Berger, F. J.; Bendel, C.; Li, H.; Flavel, B. S.; Zaumseil, J. Absolute Quantification of sp^3 Defects in Semiconducting Single-Wall Carbon Nanotubes by Raman Spectroscopy. *J. Phys. Chem. Lett.* **2022**, *13*, 3542−3548.
(50) Dresselhaus, M. S.; Jorio, A.; Souza Filho, A. G.; Saito, R. Defect Characterization in Graphene and Carbon Nanotubes Using Raman Spectroscopy. *Philos. Trans. R. Soc., A* **2010**, *368*, 5355−5377.
(51) Xhyliu, F.; Ao, G. Surface Coating- and Light-Controlled Oxygen Doping of Carbon Nanotubes. *J. Phys. Chem. C* **2021**, *125*, 9236−9243.
(52) Makuła, P.; Pacia, M.; Macyk, W. How to Correctly Determine the Band Gap Energy of Modified Semiconductor Photocatalysts Based on UV-Vis Spectra. *J. Phys. Chem. Lett.* **2018**, *9*, 6814−6817.
(53) Li, Y.; Wu, X.; Kim, M.; Fortner, J.; Qu, H.; Wang, Y. Fluorescent Ultrashort Nanotubes from Defect-Induced Chemical Cutting. *Chem. Mater.* **2019**, *31*, 4536−4544.
(54) Ziegler, K. J.; Gu, Z.; Peng, H.; Flor, E. L.; Hauge, R. H.; Smalley, R. E. Controlled Oxidative Cutting of Single-Walled Carbon Nanotubes. *J. Am. Chem. Soc.* **2005**, *127*, 1541−1547.
(55) Raynaud, C.; Claude, T.; Borel, A.; Amara, M. R.; Graf, A.; Zaumseil, J.; Lauret, J.-S.; Chassagneux, Y.; Voisin, C. Super-

https://doi.org/10.1021/acs.jpcc.3c07000
J. Phys. Chem. C 2024, 128, 2012−2021

localization of Excitons in Carbon Nanotubes at Cryogenic Temperature. *Nano Lett.* **2019**, *19*, 7210−7216.
(56) Berger, F. J.; Lüttgens, J.; Nowack, T.; Kutsch, T.; Lindenthal, S.; Kistner, L.; Müller, C. C.; Bongartz, L. M.; Lumsargis, V. A.; Zakharko, Y.; Zaumseil, J. Brightening of Long, Polymer-Wrapped Carbon Nanotubes by sp^3 Functionalization in Organic Solvents. *ACS Nano* **2019**, *13*, 9259−9269.
(57) Powell, L. R.; Piao, Y.; Wang, Y. Optical Excitation of Carbon Nanotubes Drives Localized Diazonium Reactions. *J. Phys. Chem. Lett.* **2016**, *7*, 3690−3694.
(58) Perebeinos, V.; Avouris, P. Phonon and Electronic Non-radiative Decay Mechanisms of Excitons in Carbon Nanotubes. *Phys. Rev. Lett.* **2008**, *101*, 057401.
(59) He, X.; Velizhanin, K. A.; Bullard, G.; Bai, Y.; Olivier, J.-H.; Hartmann, N. F.; Gifford, B. J.; Kilina, S.; Tretiak, S.; Htoon, H.; et al. Solvent- and Wavelength-Dependent Photoluminescence Relaxation Dynamics of Carbon Nanotube sp^3 Defect States. *ACS Nano* **2018**, *12*, 8060−8070.
(60) Kim, Y.; Velizhanin, K. A.; He, X.; Sarpkaya, I.; Yomogida, Y.; Tanaka, T.; Kataura, H.; Doorn, S. K.; Htoon, H. Photoluminescence Intensity Fluctuations and Temperature-Dependent Decay Dynamics of Individual Carbon Nanotube sp^3 Defects. *J. Phys. Chem. Lett.* **2019**, *10*, 1423−1430.
(61) Kim, M.; Adamska, L.; Hartmann, N. F.; Kwon, H.; Liu, J.; Velizhanin, K. A.; Piao, Y.; Powell, L. R.; Meany, B.; Doorn, S. K.; et al. Fluorescent Carbon Nanotube Defects Manifest Substantial Vibrational Reorganization. *J. Phys. Chem. C* **2016**, *120*, 11268−11276.
(62) Wang, Y.; Wang, Q.; Zhan, X.; Wang, F.; Safdar, M.; He, J. Visible Light Driven Type II Heterostructures and Their Enhanced Photocatalysis Properties: A Review. *Nanoscale* **2013**, *5*, 8326−8339.

https://doi.org/10.1021/acs.jpcc.3c07000
J. Phys. Chem. C 2024, 128, 2012−2021